Journal of Petroleum Science and Engineering 196 (2021) 107749

Contents lists available at ScienceDirect

Journal of Petroleum Science and Engineering

journal homepage: http://www.elsevier.com/locate/petrol

Quantitative prediction of fluvial sandbodies by combining seismic attributes of neighboring zones

Wei Li [a,b,**], Dali Yue [a,*], Luca Colombera [b], Yushan Du [c], Shengyou Zhang [a], Ruijing Liu [a], Wurong Wang [a]

[a] State Key Laboratory of Petroleum Resources and Prospecting, College of Geosciences, China University of Petroleum (Beijing), Beijing, 102249, China
[b] Fluvial & Eolian Research Group, School of Earth & Environment, University of Leeds, Leeds, LS2 9JT, UK
[c] Shengli Oil Field Company, SINOPEC, Dongying, Shandong, 257015, China

ARTICLE INFO

Keywords:
Fluvial sandbodies
Seismic attribute
Stratal slices
Seismic interference
Support vector regression
Chengdao oilfield

ABSTRACT

The geological and geophysical characterization of hydrocarbon-bearing sandstones of fluvial origin is a challenging task. Channel sandbodies occurring at different stratigraphic levels (i.e., in a reservoir interval of interest as well as in overlying and underlying stratigraphic intervals) but overlapping in planview usually cause significant seismic interference due to limitations in seismic resolution: this can produce significant error in the prediction of sand location and thickness using seismic attributes. To mitigate the effect of seismic interferences by zones neighboring a target reservoir interval, a new method is proposed that combines multiple seismic attributes of the target interval and of its interfering neighboring zones, implemented by a supervised machine learning algorithm using support vector regression (SVR). Since the thickness of neighboring intervals causing seismic interference has a constant value of a quarter of a wavelength (1/4 λ), the stratal slice corresponding with the top horizon of the target interval is taken as the base of a window of 1/4 λ to calculate seismic attributes for the overlying zone; similarly, the stratal slice corresponding with the bottom horizon is taken as the top of a window of 1/4 λ to calculate seismic attributes for the underlying zone. The proposed method was applied to a subsurface dataset (including a 3D seismic dataset and 255 wells) of the Chengdao oilfield, in the Bohai Bay Basin (China). The interval of interest is located in the Neogene Guantao Formation, whose successions are interpreted as fluvial in origin. This application demonstrates how the proposed method results in remarkably improved sandstone thickness prediction, and how consideration of multiple attributes further improves the accuracy of predicted values of sandstone thickness.

1. Introduction

Fluvial successions, which commonly host hydrocarbon reservoirs (McHargue et al., 2011; Miall, 2002), tend to be highly heterogeneous (Colombera et al., 2015; Miall, 1985; Nicholas, 2013), and usually carry a high drilling risk (Carter, 2003). Hence, prediction of sedimentary heterogeneity in fluvial reservoirs is a common but important task for petroleum geologists and geophysicists (McArdle et al., 2014; Zeng, 2018).

In the oil and gas industry, seismic attributes extracted from 3D seismic datasets are commonly employed to reveal details of reservoir architectures (Chopra and Marfurt, 2005; Mukerji et al., 2001; Zeng, 2018). To improve the accuracy of seismic attributes as tools for predicting reservoir distribution, efforts have concentrated on developing new attributes (Gersztenkorn and Marfurt, 1999; Mahob and Castagna, 2003) and on exploring integrated workflows for the effective combination of multiple attributes (Carrillat et al., 2008, 2005; Coléou et al., 2003; De Rooij and Tingdahl, 2002). In the past three decades, hundreds of seismic attributes have been developed, and some of them, such as those related to amplitude, frequency, phase and seismic texture, are ordinarily applied in reservoir characterization (Carrillat et al., 2005; Gersztenkorn and Marfurt, 1999; Mahob and Castagna, 2003; Zeng, 2010). However, only a limited number of recently developed seismic attributes determined a significant improvement in sandbody

* Corresponding author.
** Corresponding author. State Key Laboratory of Petroleum Resources and Prospecting, College of Geosciences, China University of Petroleum (Beijing), Beijing, 102249, China.
E-mail addresses: wei_li_geologist@qq.com (W. Li), yuedali@cup.edu.cn (D. Yue).

https://doi.org/10.1016/j.petrol.2020.107749
Received 22 January 2020; Received in revised form 23 June 2020; Accepted 4 August 2020
Available online 17 August 2020

prediction, compared with predictions based on established attributes (e.g., root mean square, sweetness, average peak frequency attributes) (Chopra and Marfurt, 2005; Gao, 2011; McArdle et al., 2014). Hence, some of the current research efforts are directed towards the exploration of new workflows with which to enable a more effective combination of multiple seismic attributes. For example, combinations of multiple attributes with statistical regression techniques (Carrillat et al., 2005; Gholami and Ansari, 2017), via a red-green-blue blending model (Henderson et al., 2007; McArdle and Ackers, 2012; Partyka et al., 1999, Li et al., 2019b), and using machine learning (Carrillat et al., 2008; Coléou et al., 2003; Li et al., 2019a; Veeken et al., 2009) have been widely employed in recent years. Although these integrated workflows result in improved reservoir prediction, especially in application to thin reservoir-forming sandbodies, a difficulty remains in accurately imaging sandbodies that are stacked in a way whereby they are vertically close to – though not necessarily in contact with – each other; this problem exists even when the sandbody thickness is equal to or even larger than the seismic resolution. For example, with reference to the idealized example in Fig. 1, it is difficult to map channel sandbodies contained in the middle stratigraphic interval ('layer 2' in Fig. 1) using seismic attributes, even though their thicknesses are close to or larger than a quarter of the seismic wavelength (1/4 λ), due to strong interference by the response of other sandbodies from underlying and overlying intervals (Fig. 1b) (Armitage and Stright, 2010; Bakke et al., 2013; Li et al., 2020). This is a significant problem for fluvial reservoirs composed of channel sandbodies that vary in orientation and that occur at different stratigraphic levels, but overlap in planform through their stratigraphy (Colombera et al., 2104, 2017; Ghazi and Mountney, 2009; Miall, 1988). Hence, it is imperative to develop new methods for the application of seismic attributes to better discriminate sandbodies in hydrocarbon reservoirs of fluvial origin.

Li et al. (2020) have proposed a method that for the first time applies machine learning to seismic data to mitigate the effect of seismic interference from stratigraphic intervals neighboring a zone of interest on sand-thickness prediction. The proposed method was tested by applying it to a forward seismic model of a 3D synthetic stratigraphy, whose results proved the effectiveness of considering seismic attributes of the neighboring intervals to reduce their interference and improve predictions (Li et al., 2020). Nonetheless, two limitations inherent in this method still need to be addressed, as follows: 1) only one seismic attribute was used in the original implementation of the method; 2) because seismic interference is determined by zones located above and below the target interval ('neighboring zones', hereafter) each having thickness of 1/4 λ (see below, section 3), employing the surface attributes of these zones leads to inaccurate results when their thickness is not equal to 1/4 λ. The aim of this paper is to demonstrate how these problems can be addressed. To this end, an improved workflow is proposed that combines multiple seismic attributes of the target interval and of its interference zones using machine learning with a support vector regression (SVR) algorithm.

2. Geological setting and dataset

The Bohai Bay Basin is a giant hydrocarbon province in north-eastern China, covering an area of approximately 180,000 km^2 (Fig. 2a). It mainly consists of 7 sub-basins (i.e., from east to west, the Liaohe, Liaodong Bay, Bozhong, Huanghua, Jiyang, Jizhong, and Linqing sub-basins), which have mainly formed during the Mesozoic to Cenozoic (Hou et al., 2001). The Chengning Uplift, a major positive structure in the middle Bohai Bay Basin, is flanked by the Bozhong sub-basin to the northeast, the Jiyang Sub-basin to the southeast, and the Huanghua Sub-basin to the northwest (Fig. 2a). To the northeast of the Chengning Uplift is the Chengbei Salient, which is surrounded by three depressions (the Chengbei, Shanan and Bozhong depressions) within which source rocks have accumulated.

The Chengdao oilfield is situated on the southeast edge of the Chengbei Salient (Fig. 2b). The study area is located in a proximal part of the central Chengdao oilfield, covering an area of approximately 80 km^2. The target depositional unit is the upper member of the Neogene Guantao Formation (24.6–12.0 Ma) (Fig. 2c), which has been interpreted as a fluvial succession (Li et al., 2019a, 2019b; Yue et al., 2018). Channel sandbodies contained in stratigraphic intervals referred to as 'depositional layers', and vertically separated by typically thicker (over 5 m on average) shales, were accurately imaged by Li et al. (2019a,

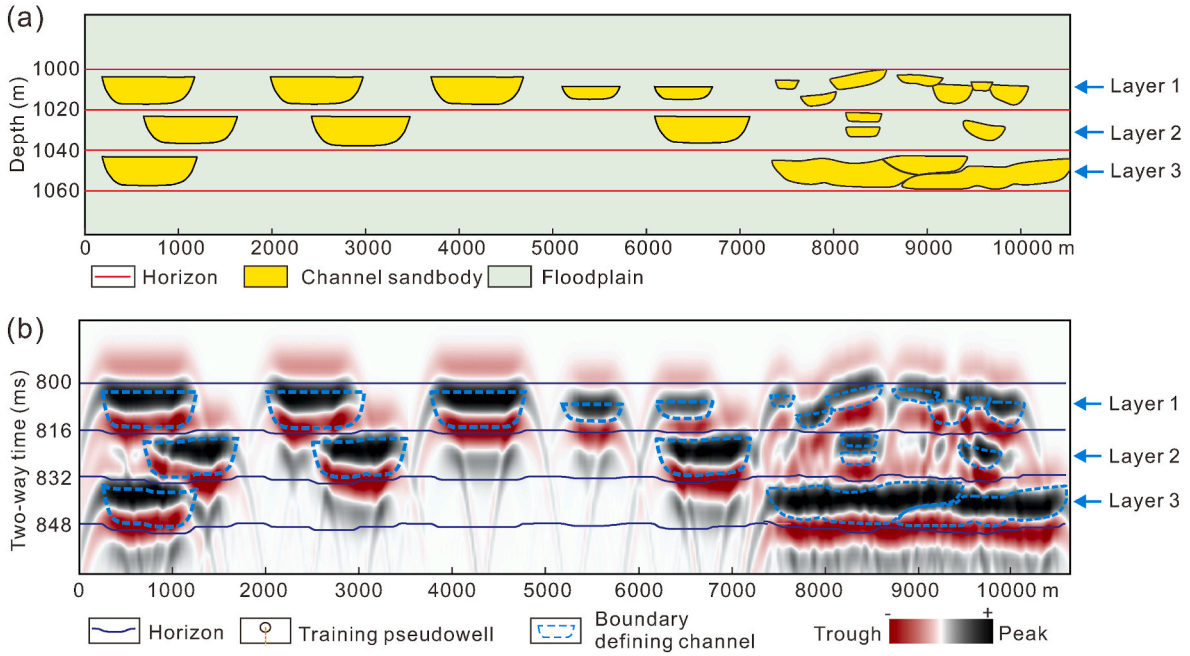

Fig. 1. (a) Lithological model used for forward seismic modelling, showing the geometry and distribution of channel sandbodies. Velocities of sandstone and mudstone are 2450 m/s and 2650 m/s, respectively. (b) The resulting synthetic seismic-reflection model, shown in a normal polarity display. The dominant frequency of the synthetic model is 38 Hz (Modified from Li et al., 2020).

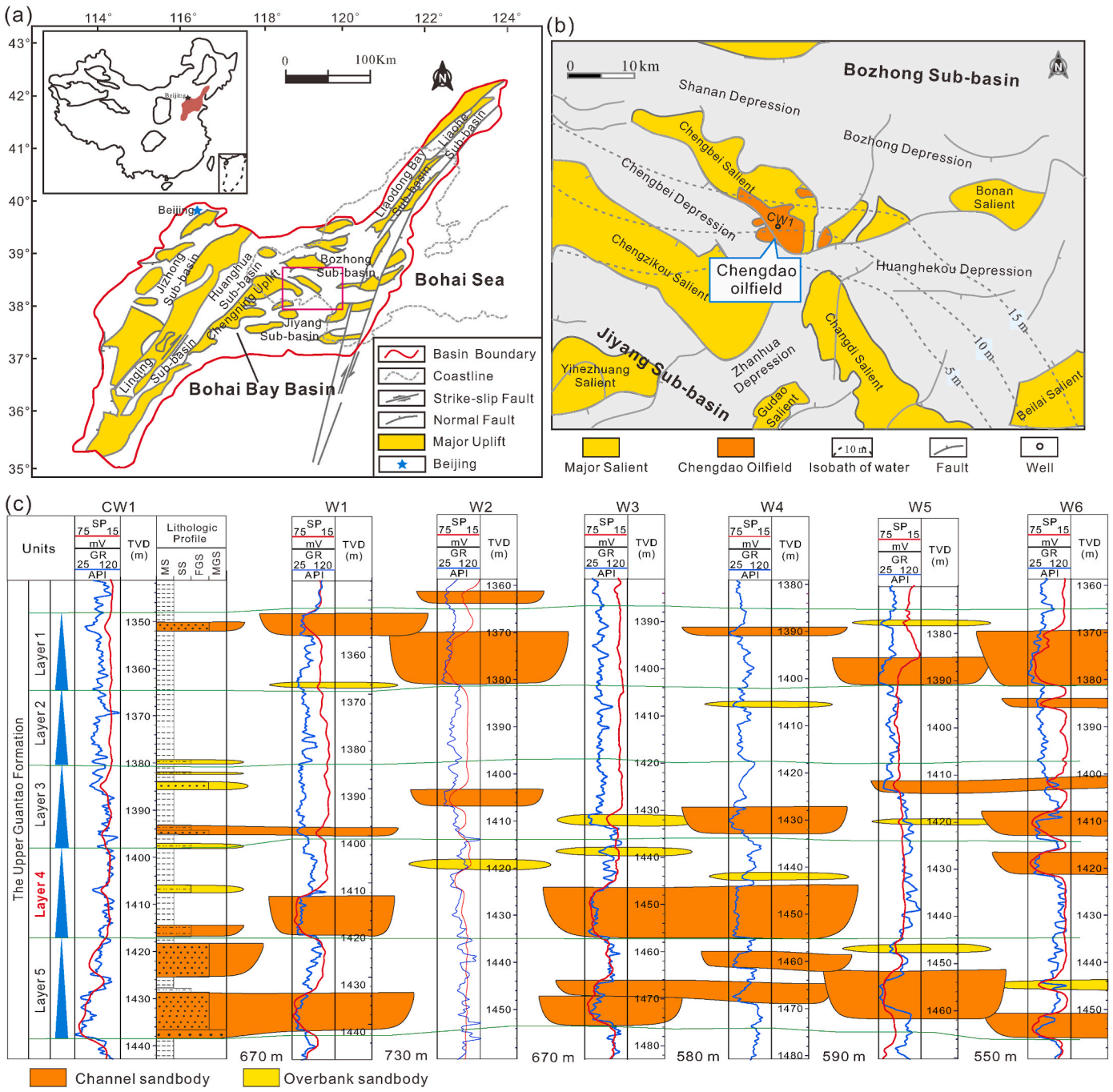

Fig. 2. (a) Location and tectonic divisions of the Bohai Bay Basin. (b) Detailed structural features of the central Bohai Bay Basin (modified from Li et al., 2019a), whose location is indicated by the red frame in Fig. 2a. (c) Well-correlation panel showing the distribution of fluvial sandbodies in the Neogene Guantao Formation. Well 'CW1' was cored. (For interpretation of the references to colour in this figure legend, the reader is referred to the Web version of this article.)

2019b) using seismic attributes. However, in other intervals where imaging of channel sandbodies is hindered by interference by sandbodies contained in stratigraphically adjacent intervals, the distribution of sandbodies could not be imaged clearly using the same seismic attributes and workflow; an example of such intervals is 'layer 4' in Fig. 2c.

The dataset that was used to predict the sandbody distribution includes 255 wells and a 3D seismic dataset. Well data comprise of different types of wireline logs, including sonic (DT), spontaneous potential (SP), gamma ray (GR), laterolog deep resistivity (LLD), and laterolog shallow resistivity (LLS); approximately half of the wells also have density (DEN) logs. In addition, seven of the wells were cored in the Neogene Guantao Formation, which is the unit of interest. The used seismic survey is a post-stack seismic dataset with a normal polarity display (Fig. 3a), covering an area of approximately 70 km^2. The dominant frequency of this post-stack seismic data is 38 Hz, and its effective bandwidth is 18–58 Hz (Fig. 3b). Spacing of both inlines and crosslines is 25 m, and the vertical sample interval is 2 ms. Statistics from the sonic logs indicate that the velocity for the successions of the Guantao Formation mainly ranges from 2350 m/s to 2700 m/s.

3. Definition of the neighboring zone and neighboring attribute slice

To better understand the interference of seismic responses and to

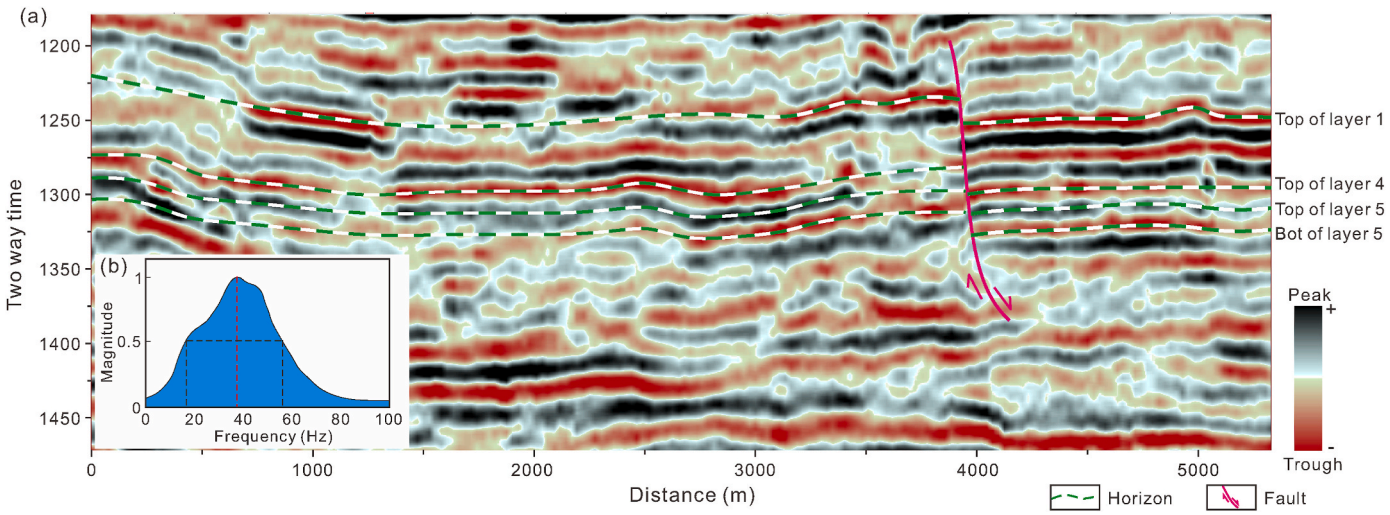

Fig. 3. (a) Seismic section extracted from the 3D seismic dataset of the study area, with a normal polarity display. The zone between tops of layer 4 and layer 5 is the interval of interest. (b) Normalized spectrum of the seismic data of the Upper Guantao Formation in the study area, showing a bandwidth of 18–58 Hz and a dominant frequency of 38 Hz.

devise a way on how best to handle these interferences for purposes of sandbody prediction, some forward seismic modelling was performed. To start, an idealized lithological model was created that incorporates sandstone bodies with rectangular and wedge geometries in cross-section, encased in mudstone (Fig. 4a). The tabular sandstone represents a unit thicker than 1/4 λ, with a constant thickness of 20 m, while the wedge-shaped (Colombera et al., 2014) sandstone (Colombera et al., 2017) has thickness varying from 0 m to 30 m. A synthetic seismic model of this lithological configuration, obtained assuming 38-Hz Ricker wavelets, indicates that significant seismic responses associated with the sandbodies are observed outside of the sandstone volumes, within a distance that is up to 1/4 λ (a two-way travel time of 1/2 T) (Fig. 4b). The forward modelling is based on the concept of 'wave front sweep velocity' (Hilterman, 1975). In addition, the seismic response of the wedge-shaped unit outside of the sandstone volume is seen over a constant vertical distance of 1/4 λ away from the sandstone top and bottom, regardless of the local thickness of the sandbody (Fig. 4b). As a result, reflections associated with the wedge-shaped unit determine interference that will affect sandbody prediction in the upper (overlying) interval. Similarly, the response of the rectangular unit will impact sandbody prediction in the lower (underlying) interval (Fig. 4b).

For post-stack seismic data, the extent of seismic response of a reflection interface depends on wavelet waveform and length (Fig. 4b) (Armitage and Stright, 2010; Bakke et al., 2013). The wavelength of the

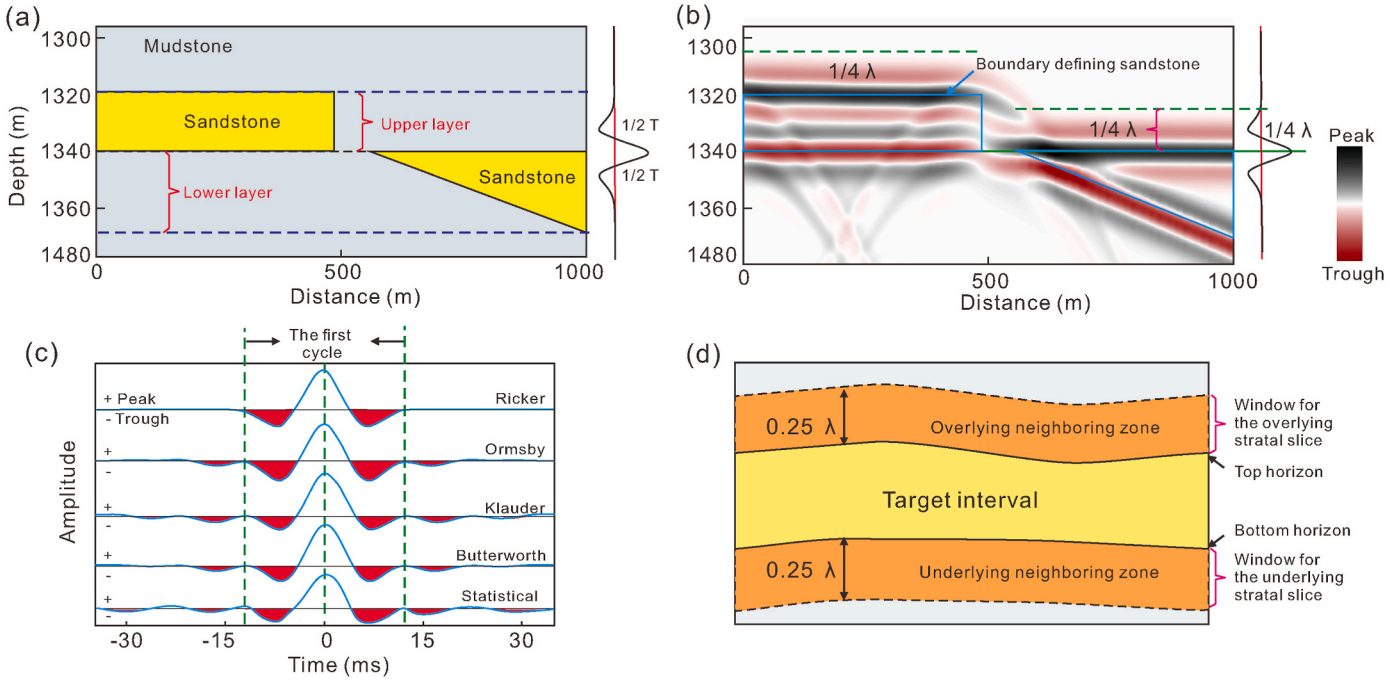

Fig. 4. (a) Lithological model used for forward seismic modelling. Velocities of sandstone and mudstone are 2450 m/s and 2650 m/s, respectively; densities of mudstone and sandstone are 2.23 g/cm^3 and 2.17 g/cm^3, respectively. (b) Synthetic seismic-reflection model. This model was convolved using the Ricker wavelets with a dominant frequency of 38 Hz, shown in a normal polarity display. (c) Waveforms for four common, theoretical, seismic wavelets, and for a statistical wavelet extracted from the seismic data of the Chengdao oilfield. (d) Sketch defining the overlying and underlying interfering neighboring zones for a target interval, each having a window of 1/4 λ.

Ricker wavelet is about a time cycle (T), whereas for other common wavelets the wavelength might correspond to several cycles or even hundreds of milliseconds (Kallweit and Wood, 1982) (Fig. 4c). Nonetheless, the first cycle shows stronger amplitude (energy) for most common wavelets (Fig. 4c). Seismic reflections (resulting from the first cycle) of a given geological unit will extend to the overlying and underlying zones over domains with a uniform height of 1/4 λ (a two-way travel time of 1/2 T) each; these domains are defined as the 'neighboring zones' discussed in this paper (orange areas in Fig. 4d).

As a consequence, seismic reflections in interfering neighboring zones may extend into a target interval. Hence, consideration of seismic responses of these neighboring zones (Fig. 4d) can help better understand seismic responses in target intervals and can be used to mitigate the effect of these interferences. Since interfering neighboring zones take a uniform thickness of 1/4 λ along the top or bottom of a target interval (Fig. 4d), stratal slices with a window of 1/4 λ above (for the overlying neighboring zone) or below (for the underlying neighboring zone) that interval are appropriate for calculation of seismic attributes of the two neighboring zones. Therefore, for the overlying neighboring zone, an attribute slice was derived as the seismic attribute calculated along the top horizon of the target interval over a window of 1/4 λ above it; similarly, for the underlying neighboring zone, an attribute slice was derived as the seismic attribute calculated along the bottom horizon of the target interval over a window of 1/4 λ below it (Fig. 4d).

4. Seismic-attribute selection using stepwise regression

Firstly, 20 types of common surface attributes were extracted for the target interval, which were related to amplitude, frequency and phase. Secondly, correlation coefficients were calculated for relationships between these attributes in areas surrounding the wells (with diameter equal to 25 m) and values of sand thickness based on well-log interpretations (Table 1). Thirdly, stepwise regression was performed between the sand thickness and the seismic attributes. During the process of stepwise regression, seismic attributes were integrated in order of their correlation coefficients, from high to low. Lastly, the three types of attributes that contribute most to the result were selected, namely, maximum peak amplitude (MPA), total amplitude (TA), and average peak frequency (APF). Statistical analyses were performed using commercial software.

The stepwise regression returns the following equation:

$$y = 0.374x_1 + 0.352x_2 - 0.159x_3 \quad (1)$$

Where y is the normalized sand thickness, and x_1, x_2 and x_3 are the normalized attributes MPA, TA and APF, respectively. The attributes MPA and TA positively correlate with sand thickness, while attribute APF shows a negative correlation with sand thickness (Table 1). Other attributes were excluded during the process of stepwise regression because they do not determine significant variation in the outcome relative to the three selected attributes (Table 2). Correlation analyses between seismic attributes indicate that the excluded attributes with correlation coefficients against sand thickness that are higher than that of APF (>0.5; Table 1) behave similarly to MPA or TA, as they show correlations with coefficients larger than 0.9 (Table 2). For this reason, consideration of these attributes does not result in significant variation in regression when MPA and TA are already considered. In part this reflects the fact that attributes MPA and TA are related to seismic amplitude, whereas attribute APF is related to seismic frequency. No seismic attributes related to seismic phase were selected because of their low correlation with sand thickness (Table 1), despite the utility of this type of attributes for imaging the margins of channel sandbodies (De Rooij and Tingdahl, 2002; Chopra and Marfurt, 2005; Li et al., 2019a).

Table 1
Twenty seismic attributes and their Pearson's correlation coefficient with sand thickness. R indicates the Pearson's correlation coefficient. Attributes are ranked in order of decreasing strength in correlation. Correlations are considered statistically signification for P-values less than 0.01 (2-tailed).

Names of seismic attributes	R for attribute vs sand thickness	P-value	Names of seismic attributes	R for attribute vs sand thickness	P-value
Max Peak Amplitude (MPA)	0.628	<0.001	Sweetness	0.491	<0.001
Total Amplitude (TA)	0.626	<0.001	Average Instant Frequency	−0.475	<0.001
Mean Amplitude	0.618	<0.001	Total Energy	0.467	<0.001
Average Peak Amplitude	0.604	<0.001	Average Energy	0.466	<0.001
Root-Mean-Square Amplitude	0.592	<0.001	Maximum Trough Amplitude	0.463	<0.001
Total Absolute Amplitude	0.554	<0.001	Instant Frequency Slope	0.444	<0.001
Average Absolute Amplitude	0.548	<0.001	Skew Amplitude	0.438	<0.001
Average Reflect Strength	0.523	<0.001	Average Trough Amplitude	0.372	<0.001
Average Peak Frequency (APF)	−0.494	<0.001	Reflect Strength Slope	−0.304	<0.001
Max Absolute Amplitude	0.494	<0.001	Average Instant Phrase	−0.118	0.059

5. Fusion of surface attributes of target interval and interfering neighboring zones

An integrated workflow is proposed that consists of five workflow elements, summarized in Fig. 5, and named A to D in temporal order of execution. Prior to the application of this workflow, wells have been tied to seismic data through synthetic seismograms and a selection of vertical seismic profiles.

Workflow element A consists in the selection of suitable seismic attributes, as detailed in section 4. In this step, seismic attributes of TA, MPA, and APF were selected from 20 common seismic attributes.

Workflow element B is the calculation of seismic surface attributes and neighboring attribute slices (Fig. 5B). The selected surface attributes were calculated between the top and bottom horizons of the target interval ('layer 4' in Fig. 2c). The upper and lower attribute stratal slices were calculated considering a window of 1/4 λ (equal to a two-way travel time of 1/2 T) parallel to the top and bottom horizons. For these stratal slices, the selected seismic attributes can be regarded as approximate surface attributes extracted along a horizon over a window of 1/4 λ (Fig. 5B).

Workflow element C consists of supervised machine learning using a Support Vector Regression (SVR) algorithm (Fig. 5C). SVR is a common class of supervised learning algorithms, which was chosen to perform training between well data and seismic attributes for two main reasons, as follows: (i) the size of the training dataset is mainly limited by the number of wells (dozens to few hundreds), and SVR has been found to be an effective algorithm for training datasets that are limited in size (Chapell and Vapnik, 2000; Cortes and Vapnik, 1995; Vapnik et al., 1997); (ii) the application of three common supervised machine learning algorithms, i.e., genetic-network, SVR and backpropagation (BP), was previously tested (Li et al., 2019a), indicating that SVR and

Table 2
Pearson's correlation coefficient between different seismic attributes. All the seismic attributes were calculated between the top and bottom horizons of layer 4 shown in Fig. 2. Abbreviation: Ave – average, Abs – absolute, Amp – amplitude, Tot – Total, Str – strength, RMS – root mean square.

	Sand Thickness	Ave Abs Amp	Mean Amp	RMS Amp	Avg Peak Freq	Avg Reflect Str	Tot Amp	Tot Abs Amp	Max Abs Amp
Sand Thickness	1.00								
Ave Abs Amp	0.55	1.00							
Mean Amp	0.62	0.76	1.00						
RMS Amp	0.59	0.91	0.90	1.00					
Avg Peak Freq	−0.49	−0.58	−0.57	−0.50	1.00				
Avg Reflect Str	0.52	0.98	0.73	0.92	−0.48	1.00			
Tot Amp	0.63	0.75	0.98	0.88	−0.56	0.71	1.00		
Tot Abs Amp	0.55	0.99	0.77	0.92	−0.58	0.99	0.75	1.00	
Max Abs Amp	0.49	0.95	0.69	0.90	−0.43	0.99	0.67	0.97	1.00

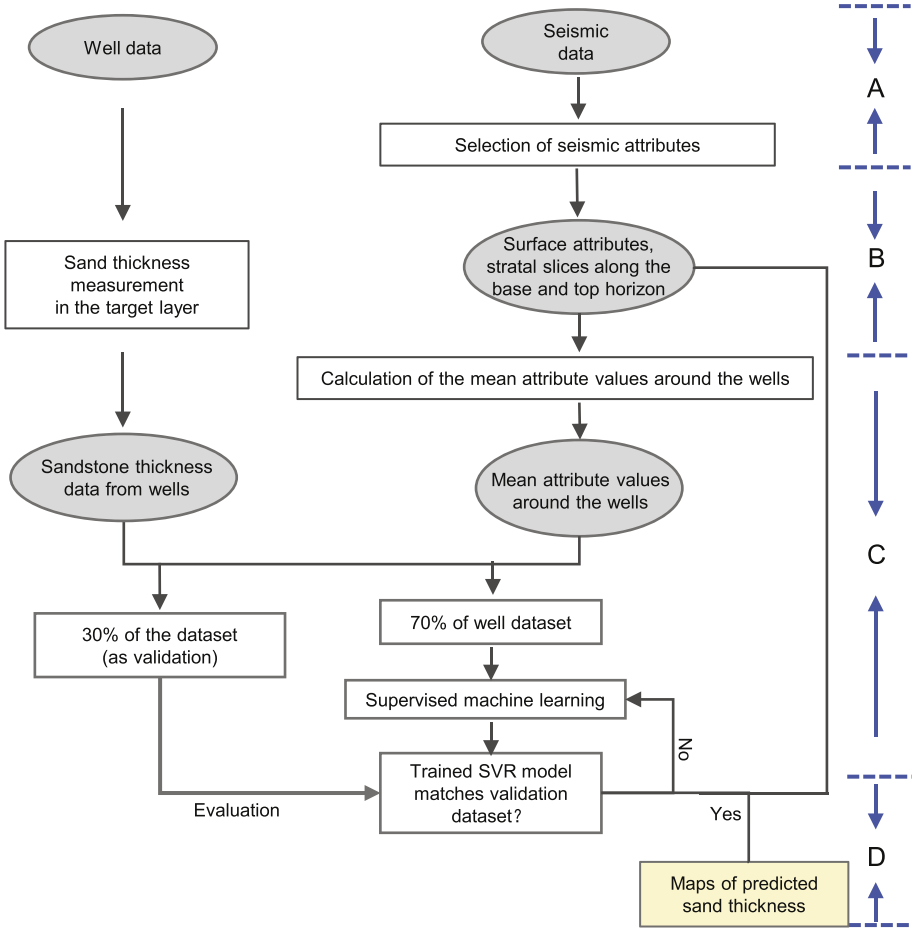

Fig. 5. Workflow diagram outlining the methodology for fusing seismic surface attributes and neighboring attribute slices. It consists of four workflow elements, labeled A to D (see text for details).

genetic-network both worked well, but SVR performed best. In this work, the radial basis function (RBF) is chosen as a kernel function (see Supporting material for chosen parameters). Values of sand thickness based on well logs and mean attribute values from domains centered on the wells and having a diameter of 25 m were input as training dataset, in which the sand thickness was the object of prediction (label). For training the machine learning algorithm, 70% of the well dataset was chosen randomly as input to the SVR. On this basis, a trained SVR model of seismic attributes and sand thickness was generated. The remaining 30% of the well data were separated for purposes of validation (see below).

Workflow element D is the last step, in which the multiple surface attributes and the neighboring attribute stratal slices were fused using the trained SVR model (Fig. 5D). The results of this step consist of the predicted sand thickness, which can be evaluated using the unused 30% of well data. This evaluation is based on the correlation coefficient between the values of sand thickness derived from the wireline logs and the corresponding sand thickness values predicted using the seismic attributes.

6. Distribution of seismic attributes and predicted sand thickness

6.1. Seismic attributes: characteristics, limitations and comparison with well logs

As mentioned above, twenty types of common seismic attributes were calculated for the target interval. Correlation analyses between the

extracted seismic attributes and sand thickness indicate that MPA (Max Peak Amplitude) returned the highest Pearson's correlation coefficient (Table 1); the attribute map for MPA in the interval of interest is shown in Fig. 6a. Attribute slices were also calculated along the top and bottom horizons within windows of 1/4 λ above and below them; stratal slices of MPA are shown for these in Fig. 6b and c.

The areas showing higher attribute values in the target interval and in the neighboring zones delineate a wider elongated belt and several narrower ribbon-like features, and some of these high-value sectors appear to have the same location and shape across the three maps (Fig. 6). This similarity in the distribution of high-value areas suggests that the seismic attributes of the target interval likely suffer from interference from seismic reflections related to the overlying and underlying neighboring zones. A comparison between the MPA attribute and well-log interpretations in the target interval indicates that the majority of wells intersecting channel sandbodies were located in areas with higher attribute values (cf. wells W1, W3, W4 and W6 in Fig. 2c). However, some of the wells that do not penetrate sandbodies, such as well W5 (see Fig. 2c), also show high values in MPA on the attribute map (see arrow in Fig. 6a). Well-log interpretation of W5 indicates that a 9.5-m channel sandbody lies below the target interval (in layer 5, Fig. 2c), in agreement with the fact that the area near W5 shows a high MPA value in the lower attribute slice (see arrow in Fig. 6c). Hence, the high values near W5 in the target intervals are thought to be due to seismic reflection of the underlying channel sandbody (channel sandbody intersected by W5 in layer 5, Fig. 2c). Where well control is lacking, however, it is not straightforward to determine whether high attribute values result from the target interval or from the neighboring zones, making it difficult to define sandbody boundaries solely on the basis of seismic attributes of the target interval.

6.2. Sand-thickness prediction

The MPA attributes in the target interval and neighboring stratal

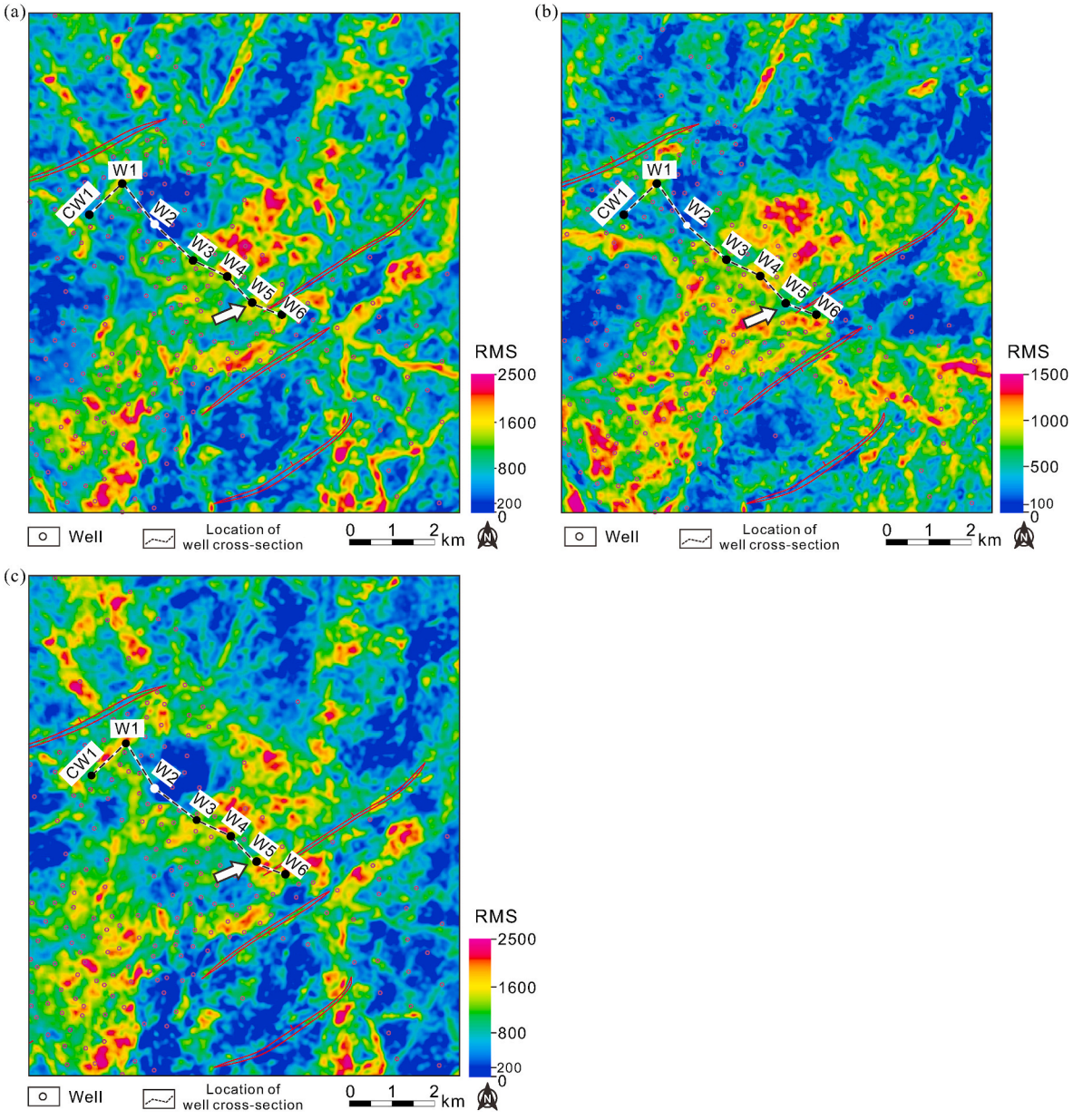

Fig. 6. (a) MPA attribute of the target interval. (b) Upper neighboring slice of MPA attribute, calculated along the top horizon of the target interval within a window of 1/4 λ above the horizon. (c) Lower neighboring slice of MPA attribute, calculated along the bottom horizon of the target interval within a window of 1/4 λ below the horizon. A well-to-well correlation panel through the labeled wells (CW1 to W6) is presented in Fig. 2c.

slices were combined and used to predict sand thickness using the SVR machine-learning algorithm, following the workflow shown in Fig. 5. Prediction results are shown in Fig. 7a. Generally, this approach based on MPA fusion returns a predicted distribution of sand thickness delineating a principal larger channel sandbody and several narrower ones; the morphologies of these sandbodies are clearer than those imaged using seismic attributes alone (Figs. 6a and 7a). To use seismic data more fully, the three selected attributes (MPA, TA and APF) of the target interval and neighboring zones were fused to obtain an alternative prediction of sand thickness (Fig. 7b). Predictions based on MPA alone and based on fusion of the three selected attributes are similar in terms of overall trends, but with differences in local predicted values.

7. Discussion

7.1. Prediction improvements, method performance and advantages

Qualitatively, a clearer map of the distribution of channel sandbodies is achieved by using the proposed method based on fused MPA attributes (Figs. 6a and 7a). A comparison of predictions against well data (well-to-well correlation panel in Fig. 2c, and Figs. 6 and 7) suggests that the proposed method can reduce interferences caused by sandbodies in neighboring zones. This is especially evident for the area around well W5, which shows a high value in MPA because of interference by the underlying zone (see section 6.1): the proposed method allows recognizing the lack of channel sandbodies in the target interval around well W5.

Quantitatively, values of predicted sand thickness using the proposed workflow yield much higher correlation with values of sand thickness as observed in the wells, in comparison with both the original seismic attribute alone and the predictions resulting from the application of the SVR algorithm without considering the neighboring zones (Table 3, Fig. 8a). Values of MPA attribute and sand thickness measured in well logs show positive correlation, with a Pearson's correlation coefficient equal to 0.628 (Table 1, Fig. 8a). Fusion of the three selected seismic attributes using the SVR machine-learning algorithm slightly improved the predicted sand thickness, with a correlation coefficient of 0.717 (Table 3). However, combining the MPA attribute of the target interval and of its neighboring zones remarkably improved the correlation between the predicted and actual sand thickness, with a correlation coefficient of 0.846 for the training wells and 0.828 for the validation wells (Table 3). In addition, the correlation coefficients for the training and validation data are similar, indicating that the trained SVR model is reasonable, and is not affected by overtraining (Table 3). Application of the same method with fusion of the three selected attributes in the target and neighboring zones further improved the accuracy of the predicted sand thickness, showing higher correlation coefficients of 0.852 (Fig. 8b) for the training wells and 0.847 (Fig. 8c) for the validation wells (Table 3).

To test the consistency of the proposed method, the workflow was performed ten times with the same parameters (see section 5) but using randomly chosen training wells (70 percent of all the wells, in total 183 wells). The limited size of the training dataset (183 training points) makes it possible to train the SVR model in few seconds using a standard desktop computer. The process of combination of the two-dimensional seismic attributes by means of the trained model is also very rapid,

Table 3
Predicted sand thickness and their Pearson's correlation coefficients with the sand thickness based on well-log interpretations. R indicates the Pearson's correlation coefficient; associated P-values report statistical significance of correlations. MPA, TA and APF are acronyms of maximum peak amplitude, total amplitude and average peak frequency, respectively.

Predicted sand thickness with different methods	R for predicted sand thickness vs actual sand thickness	P-value
Combination of MPA, TA and APF attributes in the target interval	0.717	<0.001
Combination of the MPA in the target interval and the neighboring zones (Training wells)	0.846	<0.001
Combination of the MPA in the target interval and the neighboring zones (Validated wells)	0.828	<0.001
Combination of MPA, TA and APF attributes in the target interval and the neighboring zones (Training wells)	0.852	<0.001
Combination of MPA, TA and APF attributes in the target interval and the neighboring zones (Validated wells)	0.847	<0.001

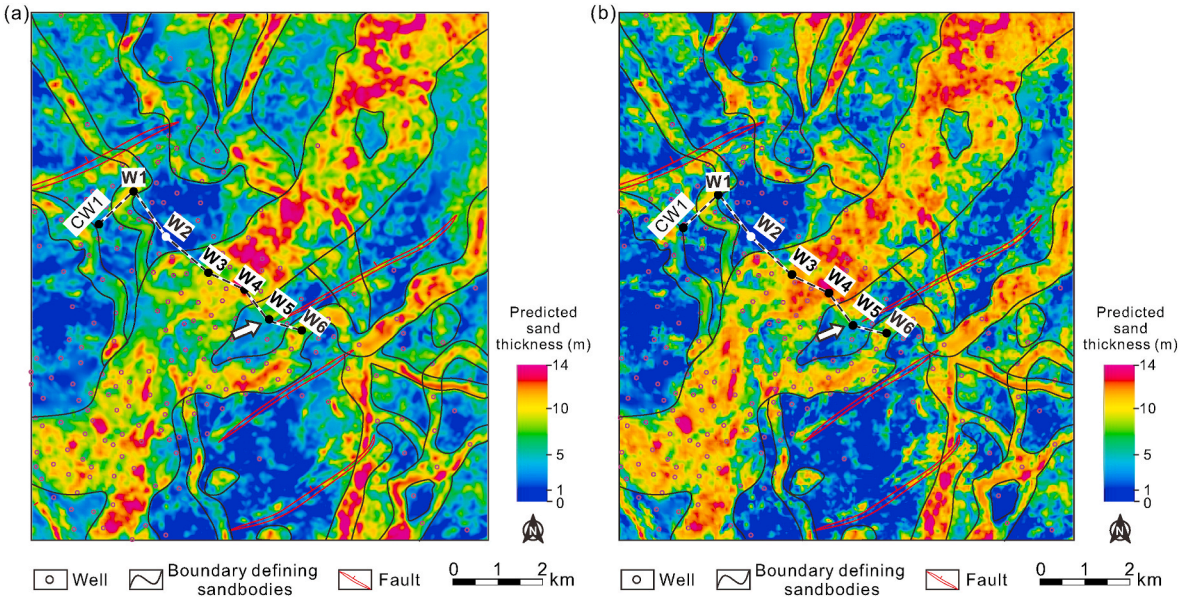

Fig. 7. Predicted sand thickness by combining the seismic surface attributes and the neighboring attribute slices. (a) Prediction based on MPA attribute only. (b) Prediction based on fusion of three seismic attributes (MPA, TA and APF). A well cross-section through labeled wells (CW1 to W6) is presented in Fig. 2c. The arrow points out a region having high MPA values in correspondence with well W5 (cf. Fig. 6a).

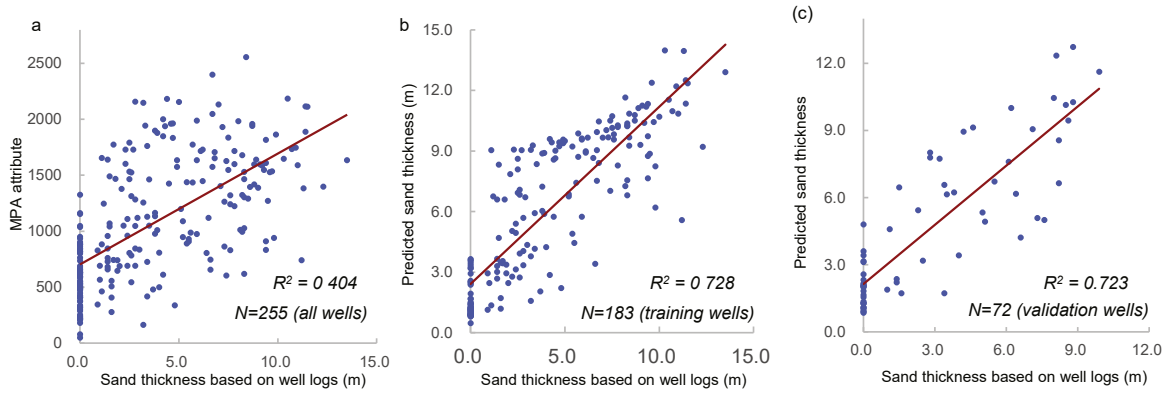

Fig. 8. Analyses of correlations. (a) Relationships between values of the MPA attribute and the sand thickness observed in well logs. (b–c) Relationships between values of sand thickness predicted by combining attributes of MPA, TA and APF and those based on well logs. (b) shows the relationship for training wells; (c) shows the relationship for validation wells.

and can usually be completed in less than 15 s, i.e. in a time that is the same order of magnitude as that required for calculation of a surface seismic attribute from the same seismic data (e.g., root mean square amplitude). The consistency of the method is demonstrated by prediction results near all the wells (255 wells, including training and validation wells): the ten different outputs show similar distributions of predicted sand thickness (Fig. 9).

In addition, for neighboring zones causing seismic interference, considering attribute slices for a window of 1/4 λ, instead of surface attributes, has two advantages. First, there is no need to interpret additional seismic horizons for the neighboring stratigraphic intervals, which reduces the workload and makes the application of the method feasible even where horizons in neighboring layers are not easily defined. Second, consideration of attribute slices for the neighboring zones improves accuracy, since considering surface attributes for stratigraphic intervals thicker than 1/4 λ leads to less accurate results.

7.2. Limitations

The combination of seismic surface attributes with neighboring attribute slices was obtained by supervised machine learning with an SVR algorithm; a necessary implication is that dozens of wells are necessary for providing a meaningful training dataset. A key factor is whether the selected wells are broadly representative of the geological features of interest, such as thickness of sandbodies and their spatial distribution in the target interval and neighboring zones. Considering the inherent variability of geological architectures of fluvial reservoirs, it is not possible to establish a specific number of wells that can be universally considered for the application of the proposed method. Nonetheless, for the example application presented herein, it has been possible to vary the number of wells used for training, through a process of random selection, to test the sensitivity of the outcome of the method to the number of wells employed (Table 4). These results provide a reference to other examples of fluvial reservoirs with comparable architectures. The similar values of correlation coefficients between the training and validation datasets indicate that the impact of the number of wells on the results is limited when the training wells are more than 75; employing 50 training wells also returns acceptable outcomes, as indicated by the high correlation shown in the validation dataset (0.816) (Table 4). For the smallest number of training wells considered (40 wells; Table 4), the discrepancy in correlation between the training and the validation datasets is relatively large (0.879 vs 0.767), meaning that the outcome of the proposed method begins to be affected by the more limited size of the training dataset. This method is therefore suitable for reservoirs with extensive well control (such as 50 or more wells for complex fluvial successions, comparable to that considered in this research), and where wells are distributed over a wide area.

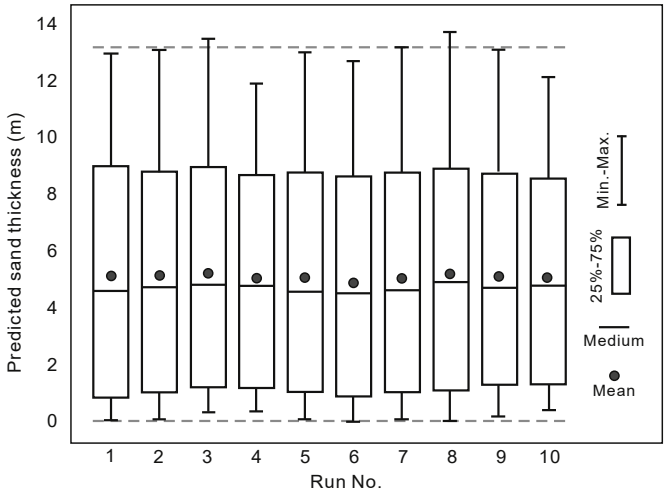

Fig. 9. Comparison of box-plots showing the predicted thickness in the target interval (layer 4 in Fig. 2c) for ten alternative predictions. The ten results were produced by the proposed method; the parameter settings of the SVR algorithm were the same, but the set of randomly chosen wells used for training (70% of all wells in all cases) differed.

Table 4
Pearson's correlation coefficients between the actual and predicted sand thickness based on a variable number of randomly selected training wells. The predicted sand thicknesses were produced by the proposed method. R indicates the Pearson's correlation coefficient; associated P-values report statistical significance of correlations.

Number of training wells	Training dataset		Validation dataset	
	R for predicted vs actual sand thickness	P-value	R for predicted vs actual sand thickness	P-value
178 wells (70% of all wells)	0.852	<0.001	0.843	<0.001
150 wells	0.848	<0.001	0.846	<0.001
100 wells	0.850	<0.001	0.842	<0.001
75 wells	0.862	<0.001	0.841	<0.001
50 wells	0.867	<0.001	0.816	<0.001
40 wells	0.882	<0.001	0.767	<0.001

8. Conclusions

For a stratigraphic interval of interest in a fluvial succession, seismic responses may be strongly interfered by responses produced by vertically neighboring zones. Commonly, interference by overlying and underlyingstratigraphic intervals is important within a window of 1/4 λ. In order to mitigate the effects of seismic interference from these neighboring zones, a method has been proposed to combine seismic attributes of a target reservoir interval and of its stratigraphically overlying and underlying zones using supervised machine learning with an SVR algorithm. This method builds upon an existing approach to produce quantitative predictions of sand thickness in the target interval using seismic data from both the interval itself and its neighboring zones. Seismic attributes for the overlying zone are derived by producing stratal slices along the top horizon of the target interval assuming a window of 1/4 λ above its top. Similarly, seismic attributes for the underlying zone are calculated by producing stratal slices along the bottom horizon with a window of 1/4 λ below its bottom.

Application of the method to a dataset consisting of 255 wells and a 3D seismic dataset proved that the combination of seismic attributes from the target layer and its neighboring zones can significantly improve the prediction of sand thickness, relative to equivalent predictions based solely on seismic attributes or on application of the SVR algorithm to the target interval alone. These improvements in prediction have been quantified by correlation coefficients between values of sand thickness predicted using the technique and sand-thickness measurements operated on well logs. This work demonstrates how this method enables the detailed mapping of the planform extent and geometry of multiple channel sandbodies.

Credit author statement

Wei Li: Conceptualization, Methodology, Software, Writing - original draft. **Dali Yue:** Resources, Supervision, Project administration. **Luca Colombera:** Term, Writing - review & editing, Supervision. **Yushan Du:** Resources. **Shengyou Zhang:** Formal analysis. **Ruijing Liu:** Formal analysis. **Wurong Wang:** Formal analysis.

Declaration of competing interest

The authors declare that they have no known competing financial interests or personal relationshipsthat could have appeared to influence the work reported in this paper.

Acknowledgments

This study was financially supported by the National Science and Technology Major Projects of China (No. 2017ZX05009001-002), the Strategic Cooperation Technology Projects of CNPC and CUPB (ZLZX2020-02), the National Natural Science Foundation Project of China (No. 41872107), Cooperation Project of the Strategic Cooperation Technology Projects of CNPC and CUPB (ZLZX2020-02), and the National Science and Technology Major Projects of China (No. 2017ZX05009001-002). We thank the Shengli Oil Field Company for providing and permitting publication of the subsurface data. LC was supported by the sponsors and partners of FRG-ERG: AkerBP, Areva (now Orano), BHPBilliton, Cairn India (Vedanta), ConocoPhillips, Chevron, Equinor, Murphy Oil, Nexen-CNOOC, Occidental, Petrotechnical Data Systems, Saudi Aramco, Shell, Tullow Oil, Woodside and YPF. We gratefully acknowledge three anonymous referees for their reviews, which have improved the article.

Appendix A. Supplementary data

Supplementary data to this article can be found online at https://doi.org/10.1016/j.petrol.2020.107749.

References

Armitage, D.A., Stright, L., 2010. Modeling and interpreting the seismic-reflection expression of sandstone in an ancient mass-transport deposit dominated deep-water slope environment. Mar. Petrol. Geol. 27, 1–12. https://doi.org/10.1016/j.marpetgeo.2009.08.013.

Bakke, K., Kane, I.A., Martinsen, O.J., Petersen, S.A., Johansen, T.A., Hustoft, S., Jacobsen, F.H., Groth, A., 2013. Seismic modeling in the analysis of deep-water sandstone termination styles. Am. Assoc. Petrol. Geol. Bull. 97, 1395–1419. https://doi.org/10.1306/03041312069.

Carrillat, A., Hunt, D., Randen, T., Sonneland, L., Elvebakk, G., 2005. Automated mapping of carbonate build-ups and palaeokarst from the Norwegian Barents Sea using 3D seismic texture attributes. In: Doré, A.G., Vining, B.A. (Eds.), Petroleum Geology Conference Proceedings. Geological Society of London, London, pp. 1595–1611. https://doi.org/10.1144/0061595.

Carrillat, A., Basu, T., Ysaccis, R., Hall, J., Mansor, A., Brewer, M., 2008. Integrated geological and geophysical analysis by hierarchical classification: combining seismic stratigraphic and AVO attributes. Petrol. Geosci. 14, 339–354. https://doi.org/10.1144/1354-079308-800.

Carter, D.C., 2003. 3-D seismic geomorphology: insights into fluvial reservoir deposition and performance, Widuri field, Java Sea. Am. Assoc. Petrol. Geol. Bull. 87, 909–934. https://doi.org/10.1306/01300300183.

Chapell, C., Vapnik, V., 2000. Model selection for support vector machines. Adv. Neural Inf. Process. Syst. 230–236.

Chopra, S., Marfurt, K.J., 2005. Seismic attributes - a historical perspective. Geophysics 70. https://doi.org/10.1190/1.2098670, 3SO–28SO.

Coléou, T., Poupon, M., Azbel, K., 2003. Unsupervised seismic facies classification: a review and comparison of techniques and implementation. Lead. Edge 22, 942–953. https://doi.org/10.1190/1.1623635.

Colombera, L., Mountney, N.P., McCaffrey, W.D., 2015. A meta-study of relationships between fluvial channel-body stacking pattern and aggradation rate: implications for sequence stratigraphy. Geology 43, 283–286. https://doi.org/10.1130/G36385.1.

Colombera, L., Mountney, N.P., Felletti, F., McCaffrey, W.D., 2014. Models for guiding and ranking well-to-well correlations of channel bodies in fluvial reservoirs. AAPG (Am. Assoc. Pet. Geol.) Bull. 98, 1943–1965. https://doi.org/10.1306/05061413153.

Colombera, L., Arévalo, O.J., Mountney, N.P., 2017. Fluvial-system response to climate change: the paleocene-eocene tremp group, pyrenees, Spain. Global Planet. Change 157, 1–17. https://doi.org/10.1016/j.gloplacha.2017.08.011.

Cortes, C., Vapnik, V., 1995. Support vector networks. Mach. Learn. 20, 273–297. https://doi.org/10.1007/BF00994018.

De Rooij, M., Tingdahl, K., 2002. Meta-attributes—the key to multivolume, multiattribute interpretation. Lead. Edge 21, 1050–1053. https://doi.org/10.1190/1.1518445.

Gao, D., 2011. Latest developments in seismic texture analysis for subsurface structure, facies, and reservoir characterization: a review. Geophysics 76, W1–W13. https://doi.org/10.1190/1.3553479.

Gersztenkorn, A., Marfurt, K.J., 1999. Eigenstructure-based coherence computations as an aid to 3-D structural and stratigraphic mapping. Geophysics 64, 1468–1479. https://doi.org/10.1190/1.1444651.

Ghazi, S., Mountney, N.P., 2009. Facies and architectural element analysis of a meandering fluvial succession: the Permian Warchha Sandstone , Salt Range , Pakistan. Sediment. Geol. 221, 99–126. https://doi.org/10.1016/j.sedgeo.2009.08.002.

Gholami, A., Ansari, H.R., 2017. Estimation of porosity from seismic attributes using a committee model with bat-inspired optimization algorithm. J. Petrol. Sci. Eng. 152, 238–249. https://doi.org/10.1016/j.petrol.2017.03.013.

Henderson, J., Purves, S.J., Leppard, C., 2007. Automated delineation of geological elements from 3D seismic data through analysis of multi-channel, volumetric spectral decomposition data. First Break 25, 87–93.

Hilterman, F.J., 1975. Amplitudes of seismic waves—a quick look. Geophysics 40, 745–762. https://doi.org/10.1190/1.1440565.

Hou, G., Qian, X., Cai, D., 2001. The tectonic evolution of Bohai basin in mesozoic and cenozoic time. Acta Sci. Nat. Univ. Pekin. 37, 845–851. https://doi.org/10.13209/j.0479-8023.2001.143.

Kallweit, R.S., Wood, L.C., 1982. The limits of resolution of zero-phase wavelets. Geophysics 47, 1035–1046. https://doi.org/10.1190/1.1441367.

Li, W., Yue, D., Wang, Wenfeng, Wang, Wurong, Wu, S., Li, J., Chen, D., 2019a. Fusing multiple frequency-decomposed seismic attributes with machine learning for thickness prediction and sedimentary facies interpretation in fluvial reservoirs. J. Petrol. Sci. Eng. 177, 1087–1102. https://doi.org/10.1016/j.petrol.2019.03.017.

Li, W., Yue, D., Wu, S., Wang, Wenfeng, Li, J., Wang, Wurong, Tian, T., 2019b. Characterizing meander belts and point bars in fluvial reservoirs by combining spectral decomposition and genetic inversion. Mar. Petrol. Geol. 105, 168–184. https://doi.org/10.1016/j.marpetgeo.2019.04.015.

Li, W., Yue, D., Wu, S., Shu, Q., Wang, W., Long, T., Zhang, B., 2020. Thickness prediction for high-resolution stratigraphic interpretation by fusing seismic attributes of target and neighboring zones with an SVR algorithm. Mar. Petrol. Geol. 113, 104153. https://doi.org/10.1016/j.marpetgeo.2019.104153.

Mahob, P.N., Castagna, J.P., 2003. AVO polarization and hodograms: AVO strength and polarization product. Geophysics 68, 849–862. https://doi.org/10.1190/1.1581037.

McArdle, N.J., Ackers, M.A., 2012. Understanding seismic thin-bed responses using frequncy decomposition and RGB blending. First Break 30, 57–66. https://doi.org/10.3997/1365-2397.2012022.

McArdle, N.J., Iacopini, D., KunleDare, M.A., Paton, G.S., 2014. The use of geologic expression workflows for basin scale reconnaissance: a case study from the Exmouth

Subbasin, North Carnarvon Basin, northwestern Australia. Interpretation 2, SA163–SA177. https://doi.org/10.1190/INT-2013-0112.1.

McHargue, T., Pyrcz, M.J., Sullivan, M.D., Clark, J.D., Fildani, A., Romans, B.W., Covault, J.A., Levy, M., Posamentier, H.W., Drinkwater, N.J., 2011. Architecture of turbidite channel systems on the continental slope: patterns and predictions. Mar. Petrol. Geol. 28, 728–743. https://doi.org/10.1016/j.marpetgeo.2010.07.008.

Miall, A.D., 1985. Architectural-element analysis: a new method of facies analysis applied to fluvial deposits. Earth-Science Rev. Elsevier Sci. Publ. B.V 22, 261–308. https://doi.org/10.1016/0012-8252(85)90001-7.

Miall, A.D., 1988. Reservoir heterogeneities in fluvial sandstones: lesson from outcrop studies. Am. Assoc. Petrol. Geol. Bull. 72, 682–697. https://doi.org/10.1306/703C8F01-1707-11D7-8645000102C1865D.

Miall, A.D., 2002. Architecture and sequence stratigraphy of pleistocene fluvial systems in the Malay Basin, based on seismic time-slice analysis. Am. Assoc. Petrol. Geol. Bull. 86, 1201–1216.

Mukerji, T., Jørstad, A., Avseth, P., Mavko, G., Granli, J.R., 2001. Mapping lithofacies and pore-fluid probabilities in a North Sea reservoir: seismic inversions and statistical rock physics. Geophysics 66, 988–1001. https://doi.org/10.1190/1.1487078.

Nicholas, A., 2013. Morphodynamic diversity of the world's largest rivers. Geology 41, 475–478. https://doi.org/10.1130/G34016.1.

Partyka, G., Gridley, J., Lopez, J., 1999. Interpretational applications of spectral decomposition in reservoir characterization. Lead. Edge 18, 353–360. https://doi.org/10.1190/1.1438295.

Vapnik, V., Golowich, S.E., Smola, A., 1997. Support vector method for function approximation, regression estimation, and signal processing. Adv. Neural Inf. Process. Syst. 281–287.

Veeken, P.C.H., Priezzhev, I.I., Shmaryan, L.E., Shteyn, Y.I., Barkov, A.Y., Ampilov, Y.P., 2009. Nonlinear multitrace genetic inversion applied on seismic data across the Shtokman field, offshore northern Russia. Geophysics 74, WCD49. https://doi.org/10.1190/1.3223314.

Zeng, H., 2010. Geologic significance of anomalous instantaneous frequency. Geophysics 75, P23. https://doi.org/10.1190/1.3427638.

Zeng, H., 2018. What is seismic sedimentology? A tutorial. Interpretation 6, SD1–SD12. https://doi.org/10.1190/INT-2017-0145.1.